1 **Eastern Pacific oxygen minimum zones: Supply paths and multi-**

2 **decadal changes**

3

4

5 Lothar Stramma[1], Gregory C. Johnson[2], Eric Firing[3] and Sunke

6 Schmidtko[1,2]

7

8 [1] Leibniz-Institut für Meereswissenschaften an der Universität Kiel, IFM-GEOMAR,

9 Kiel, Germany

10

11 [2] NOAA/Pacific Marine Environmental Laboratory, Seattle, Washington, USA

12

13 [3] University of Hawaii, Department of Oceanography, Honolulu, USA

14

15 status: 04 May 2010

16

17

18 *Corresponding author address:*

19 Lothar Stramma, Leibniz-Institut für Meereswissenschaften, Düsternbrooker Weg 20

20 24105 Kiel, Germany. E-mail: lstramma@ifm-geomar.de

21 **Abstract**

22 The supply of oxygen-rich water to the oxygen minimum zones (OMZs) of the eastern

23 North and South Pacific via zonal tropical currents is investigated using shipboard

24 ADCP and hydrographic section data. Near the equator, the Equatorial Undercurrent

25 (EUC), Northern and Southern Subsurface Countercurrents (SCCs), and the Northern

26 and Southern Intermediate Countercurrents (ICCs) all carry water that is oxygen-richer

27 than adjacent westward flows, thereby providing a net oxygen supply to the eastern

28 Pacific OMZs. The synoptic velocity-weighted oxygen concentration difference

29 between eastward and westward flows is typically 10-50 μmol kg^{-1}. Sub-thermocline

30 zonal oxygen fluxes reflect decreasing oxygen concentrations of the EUC, the SCCs, and

31 the ICCs as they flow eastward. Approximately 30-year time-series in well-sampled

32 regions of the equatorial Pacific show oxygen content decreasing as rapidly as -0.55

33 μmol kg^{-1} per year in the major oxygen supply paths of the OMZs for a 200 to 700 m

34 layer, and similar trends for a density layer spanning roughly these depths. This finding

35 is in gross agreement with climate models, which generally predict expanding OMZs.

36

37 INDEX TERMS: 4231 Equatorial Oceanography, 4512 Currents, 4513 Decadal ocean

38 variability, 4834 Hypoxic environment

39 KEYWORDS: ocean circulation, water-mass spreading, tropical Pacific Ocean, oxygen

40 minimum, oxygen time series

1. Introduction

Oxygen is a very sensitive indicator of both physical and biological change in the ocean [*Joos et al.*, 2003]. As a consequence, oxygen is a key parameter for better understanding the ocean's role in climate [*Keeling and Garcia,* 2002]. Volumes of the interior ocean that are relatively poor in oxygen are often called oxygen minimum zones (OMZs). There is no consensus on the oxygen threshold defining an OMZ. When oxygen concentrations drop below ~60 to 120 µmol kg^{-1} (hypoxic conditions) important mobile macroorganisms are stressed or die.

Horizontally extensive OMZs exist in the eastern tropical Pacific, with the lowest dissolved oxygen values found from about 100 to 900 m [*Karstensen et al.,* 2008]. The strength, vertical extent, and horizontal extent of these OMZs all decrease westwards (Figure 1). OMZ cores are located at about 10°S and 10°N, separated by higher oxygen concentrations in the equatorial region (Figure 1b). Areas with $O_2 < 1$ µmol kg^{-1} are found at 300 to 500 m in parts of the eastern Pacific, well below the suboxic ($O_2 < 5$ µmol kg^{-1}) threshold. On the isopycnal $\sigma_\theta = 26.8$ kg m^{-3} (350 to 450 m), large areas with $O_2 < 5$ µmol kg^{-1} are centered at about 12–15°N in the eastern North Pacific and 5–12°S in the eastern South Pacific (Figure 2b). Lowest oxygen concentrations south of the equator are found beneath the Peru Current off northern Peru and north of the equator beneath the eastern Pacific warm pool off the coast of SW Mexico [*Fiedler and Talley,* 2006]. Similar OMZs exist in the eastern Atlantic, but they are not suboxic, having relatively high minimum dissolved oxygen concentration values: about 40 µmol kg^{-1} in the North Atlantic and 20 µmol kg^{-1} in the South Atlantic.

66   A prominent feature of ventilated thermocline models [*Luyten et al.,* 1983] is the

67   poleward deflection of streamlines toward the eastern boundary in the equatorward limbs

68   of the subtropical gyres.   This pattern leaves unventilated tropical shadow zones

69   extending westward from the eastern boundary between the equatorward edges of the

70   subtropical gyres. The predicted shadow zones roughly coincide with the tropical OMZs

71   and with maxima in CFC-derived water age [*Fine et al.,* 2001, their Figure 4]. Hence a

72   direct supply of oxygen from the subtropical gyres to the OMZs is blocked, leaving

73   eastward tropical currents as the most likely lateral advective sources of oxygen to the

74   OMZs. In the Atlantic, the North Equatorial Countercurrents and the North Equatorial

75   Undercurrent have been identified as supplying relatively oxygen-rich water to the North

76   Atlantic OMZ [*Stramma et al.,* 2008a].   Here we assess which of the many zonal

77   currents in the tropical Pacific may resupply the Pacific OMZs.

78

79   Since the OMZs primarily lie below the pycnocline, we focus on eastward currents with

80   sub-pycnocline expressions. However, the upper bounds of the OMZs do lie in the

81   density range of the Subtropical Cells. These cells connect the subtropical subduction

82   regions of both hemispheres to the eastern, equatorial upwelling regimes by equatorward

83   thermocline and poleward surface flows, together with low-latitude eastward currents

84   [*Schott et al.,* 2004]. The most germane of these eastward currents are discussed below.

85

86   The most prominent eastward current with a sub-pycnocline expression is the Equatorial

87   Undercurrent (EUC; Figure 2), which flows eastward along the equator across the entire

88   Pacific [*Johnson et al.,* 2002] carrying relatively oxygen-rich water [*Wyrtki and*

89   *Kilonsky,* 1984].   A westward Equatorial Intermediate Current (EIC) is often found

90 below the EUC in the western Pacific. The Pacific subsurface countercurrents (SCCs,

91 also known as Tsuchiya jets in the Pacific and as the North and South Equatorial

92 Undercurrents in the Atlantic) [*Tsuchiya,* 1975] are narrow eastward currents that

93 bracket the equator just below the equatorial thermocline. (The terms thermocline and

94 pycnocline – or thermostad and pycnostad – are used interchangeably here, depending

95 on historical context, since salinity plays a small role in stratifying the tropical Pacific.)

96 Deeper, denser, and weaker than the EUC, the SCCs form the poleward boundaries of

97 the 13°C equatorial thermostad discussed below. The northern SCC (NSCC) and the

98 southern SCC (SSCC), also referred to as the NSSCC and SSSCC [*Kessler,* 2006], start

99 around 3° from the equator in the western Pacific, then gradually diverge and shoal to

100 the east, with cores around 6° from the equator and 150 m below the surface by 110°W

101 [*Johnson and Moore*, 1997; *Rowe et al.,* 2000]. Another eastward current, the

102 Secondary SSCC, is found poleward of the SSCC and extending to greater densities

103 [*Rowe et al.,* 2000]. No North Pacific counterpart to the Secondary SSCC has been

104 identified. *Firing et al.* [1998] described a westward South Equatorial Intermediate

105 Current (SEIC) and a North Equatorial Intermediate Current (NEIC) centered around

106 500 m and 3° from the equator. Even deeper, denser, and weaker eastward current

107 extrema (North and South Intermediate Countercurrents; SICC, NICC) are found at

108 about 2° from the equator from 500 to 1500 m [*Firing et al.,* 1998]. These intermediate

109 countercurrents could also supply oxygen to the OMZs.

110

111 The sources, variability, and fate of many of these currents remain unresolved. For

112 instance, there is evidence that part of the EUC flows southeast into the Peru

113 Undercurrent and contributes to the coastal upwelling, but observations are sparse

114 [*Kessler,* 2006, and references therein]. The Galapagos Islands at and just south of the

115   equator at 90-92°W are a topographic barrier for the EUC and for the westward-flowing

116   South Equatorial Current (SEC) [*Eden and Timmermann,* 2004], complicating the

117   currents in the eastern equatorial Pacific. The density of the SCCs decreases

118   substantially to the east, indicating some unknown combination of diapycnal flow and

119   lateral exchange with westward recirculations [*Rowe et al.,* 2000].

120

121   South of the equator the surface-intensified South Equatorial Countercurrent is weak and

122   found mainly in the western Pacific [e.g. *Eldin,* 1983] and distinct from the SSCC. In

123   contrast, north of the equator, the NSCC is connected to the North Equatorial

124   Countercurrent (NECC). A boundary between these two currents has been set at $\sigma_\theta =$

125   25.0 kg m^{-3} in the eastern Pacific [*Hayes et al.,* 1983]. The NSCC and the SSCC cores

126   lie within the neutral density range $26.2 < \gamma_n < 26.5$ kg m^{-3} in the eastern Pacific [*Rowe*

127   *et al.*, 2000]. (Here we use σ_θ, which is close to γ_n in the region of interest; the depth of

128   26.2 kg m^{-3} for these quantities is the same within a few meters, and for 26.5 kg m^{-3} σ_θ is

129   deeper than γ_n by as much as 30 m. Hence our analysis covers a slightly larger depth

130   interval than that of *Rowe et al.* [2000]). The climatological oxygen distribution on $\sigma_\theta =$

131   26.3 kg m^{-3} (about 150 to 300 m; Figure 2a), near the NSCC and SSCC cores, shows no

132   enhanced values at the latitudes of the SCCs (3-6° from the equator). The spatial

133   smoothing and temporal averaging in the climatology may mask the narrow structure

134   associated with the Pacific SCCs. Similar plots in the Atlantic, however, (not shown) do

135   contain a hint of oxygen-rich structure associated with the SCCs.

136

137   The OMZ is influenced by several water masses. The oxygen-rich surface waters lie

138   atop the OMZ and contrast with it. The Subtropical Underwater (STUW) carried

139   eastward into the upper OMZs by the EUC is also relatively oxygen-rich compared to

140   the OMZ. The 13°C Equatorial Water (13CW) [*Montgomery and Stroup*, 1962] and the

141   South and North Pacific Eastern Subtropical Mode Water (SPESTMW, NPESTMW)

142   [*Hanawa and Talley*, 2001; *Wong and Johnson*, 2003]) all move eastward in the deep

143   EUC and SCC's, carrying oxygen-richer water to the OMZ. The Antarctic Intermediate

144   Water (AAIW), oxygen-richer than the North Pacific Intermediate Water (NPIW)

145   [*Wijffels et al.,*1996] is also carried eastward in the deeper reaches of the SCC's and the

146   ICC's.

147

148   Climate and biogeochemical models predict an overall decline in ocean dissolved

149   oxygen concentrations and a consequent expansion of OMZs under global warming

150   conditions [*Matear and Hirst*, 2003; *Oschlies et al.* 2008]. Only a few reports of multi-

151   decadal ocean oxygen changes have been made, however. For example, declining

152   oxygen concentrations have been observed in the interior waters of the eastern subarctic

153   Pacific at Ocean Station Papa (50°N, 145°W) [*Whitney et al.,* 2007] as well as for

154   several subtropical areas in all oceans [*Emerson et al.,* 2004; Table 1]. Long records of

155   dissolved oxygen are sparser in the tropical Pacific than at higher latitudes. Recently

156   *Stramma et al.* [2008b] described declining oxygen concentrations in the low oxygen

157   layers of all tropical oceans. Here we investigate the supply routes of oxygen-rich water

158   to the OMZs of the eastern North and South Pacific, estimate zonal sub-thermocline

159   oxygen fluxes for the equatorial Pacific between 8°S and 8°N in isopycnal layers as well

160   as for some of the currents that supply oxygen to the OMZs, and present oxygen time

161   series for some equatorial areas with sampling sufficient to describe multi-decadal

162   changes.

163

2. Instruments and Methods

2.1. Hydrographic and shipboard ADCP data

Shipboard hydrographic and current observations from meridional cross-equatorial sections occupied by the World Ocean Circulation Experiment (WOCE) and the Tropical Atmosphere-Ocean (TAO) project are used here to study zonal supply paths of oxygen-rich water to the OMZs in the Pacific. The WOCE data include high-quality full-depth vertical profiles of temperature, salinity, and dissolved oxygen versus pressure from a CTD/O_2 (Conductivity-Temperature-Depth-Oxygen) instrument calibrated by water sample analyses, upper water-column current data from a shipboard ADCP (Acoustic Doppler Current Profiler), and full water-column currents from a lowered ADCP in some locations [*Firing et al.*, 1998]. The TAO project has maintained an array of approximately 70 moorings in the equatorial Pacific since the 1990s. Maintenance operations have routinely included meridional sections with 1000-m CTD stations and shipboard ADCP data. On a few of these TAO cruises, dissolved oxygen was measured as well. Data from some of the TAO sections with oxygen measurements and shipboard ADCP measurements will be analyzed here.

The westernmost TAO sections analyzed here, along 170°W, were occupied by NOAA Ship *Ka'imimoana* in July 2004 and June 2006. *Ka'imimoana* sections including oxygen measurements along 140°W were occupied in September 2004 and January 2006, and sections along 125°W were occupied later during the same cruises in September 2004 and January–February 2006.

188 We use a TAO section made in June–July 2004 along 155°W for oxygen flux

189 computations. TAO sections with oxygen sampling were occupied along 110°W in

190 October 2000, November 2003, April 2005 and April 2006. These data contribute to

191 time series constructed here and presented below. In December 2007 and January 2008

192 ADCP as well as CTD with oxygen samples were collected on a *Ronald H. Brown* cruise

193 along 110–103°W and these data are used here for oxygen flux computations as well as

194 for the time series. In October–November 2003 a TAO section including oxygen

195 sampling along 95°W was occupied on the NOAA Ship *Ronald H. Brown* from 12°N to

196 8°S, but shipboard ADCP measurements reached only about 350 m. TAO sections

197 along 95°W from October 2000, April–May 2005 and April 2006 are also used below as

198 part of an oxygen time series.

199

200 A WOCE section, designated P19, was occupied on the *R/V Knorr* in February–April

201 1993 with closely spaced full-depth stations across the equator from southern Chile to

202 Guatemala. The section runs along a nominal longitude of 88°W in the South Pacific,

203 but shifts to 85°W in the equatorial Pacific [*Tsuchiya and Talley,* 1998]. The shipboard

204 ADCP reached a maximum depth of 493 m. Lowered ADCP data were collected north

205 of 5°S and are used here to extend the vertical range of shipboard ADCP data.

206

207 **2.2. Time series**

208 Oxygen time-series are limited by the sparseness of ocean oxygen measurements. To

209 construct oxygen time series in selected areas we used the HydroBase-2 programs and

210 data set [*Curry,* 1996] including the quality-controlled historical hydrographic data base

211 WOD05 [*Boyer et al.,* 2006], and supplemented it with more recent data. As older data

212   are sparse and their accuracy more questionable, we start the time series in 1975. To

213   extend the time series towards the present, areas where recent sections with oxygen

214   measurements from the TAO project exist were selected. The areas were centered on the

215   TAO sections to minimize geographical bias. Linear trends were fitted and 95%

216   confidence intervals computed following *Stramma et al.* [2008b].

217

218   **3. Results**

219

220   **3.1. Zonal currents and the oxygen supply in the tropical Pacific**

221   There can be no net time-mean advection of oxygen by time mean currents across a

222   time-mean closed surface of a chosen oxygen concentration (oxygen isosurface)

223   bounding the OMZ. However, since no synoptic hydrographic section is likely to follow

224   all, or even much of such a surface (Figure 1), or capture time-mean conditions, there are

225   oxygen transports across the sections analyzed here. Along 170°W in July 2004, oxygen

226   concentrations exceed 60 μmol kg^{-1} in the eastward-flowing EUC, SSCC and NSCC

227   (Figure 3). In this section the EUC, SSCC, NSCC, and NECC are all connected (not

228   separated by westward flow). Below 200 m, lower oxygen values are associated with

229   the westward flow of the EIC and with bands of westward flow at 3–5°S and 4–6°N. At

230   this longitude σ_θ = 26.2 and 26.5 kg m^{-3}, which roughly bound the SCC cores in the

231   eastern Pacific, are separated by less than 50 m, except for a spreading to 80 m in the

232   lower part of the EUC and the upper EIC. The major zonal transports for 26.2 < σ_θ <

233   26.5 kg m^{-3} are found within the secondary SSCC, the southern part of the EUC, and the

234   NSCC (Figure 3b). The velocity cores of the two SCCs are denser than σ_θ = 26.5 kg m^{-3}

235   in the central Pacific, and the SSCC carries oxygen-rich water eastward, as does the

236   EUC in the upper ocean. The NSCC caries oxygen-rich water in its upper layer, but

237   below 300 m the NSCC is partly influenced by an admixture of oxygen-poor water

238   (likely from the north, given its low salinity signature).

239

240   Further east, along 140°W in January 2006, the eastward-flowing EUC, SSCC, and

241   NSCC are separated by strong westward-flowing branches of the SEC (Figure 4). The

242   thickness of $26.2 < \sigma_\theta < 26.5$ kg m^{-3} increases to more than 150 m, especially between

243   4°S and 3°N. Dissolved oxygen content along 140°W is lower compared to 155°W (the

244   gray shading scale is identical for Figures 4 to 7, but different for Figure 3), with much

245   lower oxygen in the westward flow between 2 and 4°S and north of 6°N. The SCCs still

246   have higher oxygen concentrations in their cores, but some admixture of oxygen-poor

247   water from the neighbouring westward flow is obvious below the current cores. The

248   current cores at 140°W are located within $26.2 < \sigma_\theta < 26.5$ kg m^{-3}, contrasting with

249   170°W. The NICC and especially the SICC carry relatively oxygen-rich water eastward

250   at 400 to 600 m.

251

252   Along 125°W in January–February 2006 (Figure 5), the NSCC is strong, as is the

253   NECC, to which it is connected. The NSCC core also carries relatively oxygen-rich

254   water.   South of the equator, the SSCC is strongly influenced by the surrounding

255   oxygen-poor water. While the NICC is weak in this section, the SICC is well developed,

256   carries relatively oxygen-rich water eastward, and hence is a deep provider of oxygen-

257   rich water to the OMZ. The EIC is well developed in this section, centered at about 350

258   m, and carries oxygen-poor water westward. In contrast, in the nearly contemporaneous

259   140°W section, the EIC is absent. The large changes in strength or even absence of the

260   deeper currents like the EIC, SICC, and NICC from section to section shows that the

261   variability of these currents is near their mean magnitude.

262

263   Along 95°W in November 2003 (Figure 6), the shipboard ADCP only measured currents

264   in the upper 350 m. The well oxygenated surface layer is separated from the oxygen-

265   poor layers of the OMZ below near $\sigma_\theta = 25.6$ kg m^{-3}. The EUC transports relatively

266   oxygen-rich water eastward (Figure 6b). The SEC branches found poleward of the EUC

267   in both hemispheres recirculate this relatively oxygen-rich water from the EUC

268   westward. The SSCC at about 6°S is located in the OMZ, but its core at 250 to 350 dbar

269   carries slightly oxygen-rich (but much poorer than the EUC and SEC(S)) waters

270   eastward at 250 to 300 m. The NSCC at 6°N separates the oxygen-richer water of the

271   equatorial region from the oxygen-poor water to the north. The two small westward

272   current bands at 7 and 8°N just below the NECC carry oxygen-rich water, and hence

273   might be transient recirculations of oxygen-enhanced equatorial water masses. In the

274   north a thick layer of oxygen-poor water is found under the Costa Rica Dome. Near the

275   equator the oxygen-poor layer covers only the depth range 300 to 500 m. At 500 to 800

276   m the oxygen content rises, apparently connected to the eastward flow near the equator

277   and presumably the SICC and NICC measured at about 2°S and 3°N.

278

279   The OMZs of the eastern South and North Pacific along 85°W were entirely sampled in

280   March and April 1993 (Figure 7). The southern limit of the South Pacific OMZ is near

281   18°S. The South Equatorial Current (SEC) and the Humboldt Current between 15 and

282   10°S carry oxygen-poor water from the OMZ westwards. The SCCs also carry

283   relatively oxygen-poor water eastward, leaving the deep EUC as a major source of sub-

284   thermocline oxygen-rich water at this longitude. Higher oxygen values are found in the

285   SICC and NICC at about 2°S and 2°N near 500 m. (The eastward flow on the equator

286   from 200 to 400 m also has slightly elevated oxygen, but is mostly too dense to be

287   considered part of the EUC.) North of 5°N very oxygen-poor waters span a wide depth

288   range centered near 500 m, and the eastward component of the Costa Rica Dome (CRD)

289   carries oxygen-poor water northeastwards.

290

291   The mass transports and oxygen fluxes of the eastward near-equatorial currents are

292   highly variable from one synoptic section to the next (Table 1); the variability is of the

293   same magnitude as the mean currents. Hence it is difficult to discern a clear zonal trend

294   in either variable.   Nonetheless, there is a suggestion of a decrease to the east,

295   particularly in the eastern part of the domain. Dividing the mass transport by oxygen

296   flux yields a transport-weighted oxygen concentration, and this quantity does decrease

297   systematically from west to east, as expected from the climatological oxygen

298   distribution.

299

300   Oxygen concentrations of the net eastward and westward flows in the tropical Pacific

301   between 8°S and 8°N for selected density layers (Figure 8) reveal several patterns

302   despite the strong variability in the synoptic meridional cross-equatorial sections

303   analyzed here.   Again as expected, these velocity-weighted oxygen concentrations

304   generally decrease from west to east in all layers. Except at 95°W, as discussed below,

305   velocity weighted oxygen concentrations for the eastward flow are higher (by 2 to 51

306   μmol kg^{-1}) than those for westward currents in all the density layers. Hence the eastward

307   flows supply oxygen-richer waters to the OMZs while the westward flows remove

308   oxygen-poorer water. The concentration differences between eastward and westward

309   flow generally decrease in magnitude with increasing density.   While some of the

310   lightest layer is within the thermocline, and may intersect with only the top of the OMZ,

311   the second lightest layer, which captures some of the SCCs, certainly feeds the OMZ, as

312   do the two densest layers. The largest differences in velocity-weighted oxygen

313   concentrations for eastward and westward flow are found at 140°W, near the edge of the

314   OMZs, and they generally decrease from there eastward. In the anomalous 95°W

315   section westward flow is weak and concentrated on the SEC with relatively high oxygen

316   (Figure 6), perhaps derived from the relatively oxygen-rich EUC, while the eastward

317   flow shows lower oxygen concentration (Figure 8) owing to low oxygen concentrations

318   in the SSCC and NSCC (see Figure 6).

319

320   **3.2. Oxygen time series**

321   To begin to address the difficult question of multi-decadal temporal variability of

322   oxygen concentration near the equator, recent TAO section data are combined with

323   historical data. Since the tropical Pacific OMZs do not exhibit strong seasonality

324   [*Paulmier and Ruiz Pino*, 2009], oxygen data are used here regardless of the season in

325   which they are collected.

326

327   Annual mean 200 to 700 m dissolved oxygen time series since 1975 are constructed for

328   regions from 3°S to 3°N centered on four TAO longitudes. A depth layer is chosen,

329   rather than a density layer, to include any vertical expansion or other shifts of the OMZ.

330   These regions cover the area of the major oxygen supply path for the eastern tropical

331   Pacific OMZs. All four selected areas show decreasing oxygen (Figure 9) over the last

332   30 years. Linear fits estimate trends of oxygen concentrations from -0.55 to -0.32 μmol

333   kg^{-1} a^{-1}. Trends at 165–175°W, 105–115°W, and 90-100°W are significantly different

334   from zero at 95% confidence (Table 2). Time-series for larger geographical regions

335   containing areas a) and c) of figure 9 [*Stramma et al.*, 2008b] are noisier than those

336   presented here, perhaps because they include data from larger areas, resulting in aliased

337 sampling of spatial variability (Figure 2).

338

339 Temporal trends of dissolved oxygen time series for the density layer $26.2 < \sigma_\theta < 27.18$

340 kg m^{-3} are similar to those for the 200-700 m layer (Table 2). This density layer

341 approximately spans 200 to 700 m in the equatorial Pacific (Table 2), but because

342 isopycnals are not level, the correspondence cannot be exact. For example, the mean

343 density layer oxygen values are slightly lower than those for the depth layer at 165°-

344 175°W (Figure 9a), because on the western side of our investigation area $\sigma_\theta = 26.2$ kg m^{-}

345 ^{3} is located at about 250 m depth, so here the density layer chosen excludes some the

346 relative high oxygen values between 200 and around 250 m. There are no obvious

347 temporal trends of bounding isopycnal depths in any of the study areas. The similarity

348 between the oxygen trends for these depth and density layers reinforces the hypothesis of

349 a loss of oxygen from the tropical thermocline.

350

351 Variability on shorter time-scales or larger spatial scales may influence or alias the linear

352 trends computed here. The data do not resolve shorter time-scales well. Nonetheless, in

353 three out of four areas studied linear trends for the depth layer are statistically different

354 from zero at 95% confidence. Linear trends and their 95% confidence intervals were

355 estimated using least squares procedures [e.g. *Wunsch*, 1996], and these trends account

356 for 26 to 54% of the total variance (Table 2). Degrees of freedom used to compute the

357 confidence intervals were estimated using integral time-scales [e.g. *von Storch and*

358 *Zwiers,* 1999]. One of the longest time series of oxygen, although far from the OMZ,

359 has been maintained at Ocean Station Papa in the North Pacific at 50°N. This 50-year

360 time series shows the influence of both short-term (few year to bi-decadal) atmospheric

361 or oceanic circulation oscillations and a persistent multi-decadal climate trend [*Whitney*

362   *et al.,* 2007]. El Niños might influence oxygen concentrations in the tropical Pacific.

363   During El Niño, equatorial Kelvin waves transit the eastern equatorial Pacific, deepening

364   the thermocline, which in turn, potentially deepens and partially erodes the oxycline

365   [*Fuenzalida et al.,* 2009]. After 1975, strong El Niños occurred in 1982-83, 1991-92

366   and 1997-98. Within the limits of the sampling, there are no clear oxygen decreases

367   associated with these years in the time series. These considerations notwithstanding,

368   there does appear to be evidence for a reduction of oxygen values in the zonal equatorial

369   oxygen supply path for the Pacific OMZs.

370

371   **4. Discussion and Summary**

372   In the tropical Pacific all westward currents remove oxygen-poor water from the OMZs

373   while the eastward zonal currents with a subthermocline expression supply oxygen-

374   richer water to the OMZs, including (from shallow to deep), the EUC, the SCCs, and the

375   ICCs. At the core layer of the SCCs ($26.2 < \sigma_\theta < 26.5$ kg m^{-3}; Table 1) the lower reaches

376   of the EUC and the SCCs/NECC carry oxygen-rich 13CW eastwards (Figure 2a).

377   Despite their large variability the NICC and SICC (Figure 2b) are major supply paths at

378   intermediate depth in the Pacific carrying oxygen-rich AAIW eastward. While the ICCs

379   have lower oxygen fluxes than the SCCs, they have higher oxygen values in the Eastern

380   Pacific. In the far eastern (85°W) tropical Pacific, well within the OMZs, the SCCs

381   carry relatively oxygen-poor water.

382

383   These findings contrast with the eastern North Atlantic where the NEUC/NECC is a

384   strong oxygen contributor to the OMZs even in the eastern reaches of the Atlantic

385   [*Stramma et al.,* 2008a]. Although the North Pacific OMZ is stronger than the South

386   Pacific OMZ, the NSCC carries a higher oxygen load than the SSCC. This difference

387   may be related to the higher volume transports in the NSCC compared to the SSCC

388   [*Rowe et al.,* 2000]. The eastward decrease in oxygen is well represented in the oxygen

389   fluxes of the EUC, the SCCs, and the ICCs. One reason for the weak oxygen values in

390   the SCCs in the far eastern Pacific may be that the SCCs rise in depth and decrease in

391   density from west to east, so only a fraction of the water in the eastern SCCs can have

392   arrived directly following isopycnals from the west; meridional and diapycnal exchanges

393   must be involved [*Rowe et al.*, 2000].

394

395   In a steady state ocean, the oxygen distribution at any given point is determined through

396   an equilibrium between oxygen flux divergences and consumption (respiration) through

397   biogeochemical processes [e.g. *Wyrtki*, 1962]. At higher latitudes most of the oxygen

398   loss may be biologically mediated through links between heating and stratification

399   [*Keeling and Garcia,* 2002]. However, the geographical location of the tropical Pacific

400   OMZ appears to be determined to first order by patterns of upwelling, regions of general

401   sluggish horizontal transport at the eastern boundaries, and to a lesser extent by regions

402   with high productivity as indicated through ocean color data [*Karstensen et al*., 2008].

403   With our relatively sparse data set it is not possible to determine whether biological or

404   circulation changes cause the oxygen decrease in the equatorial area in the face of highly

405   variable currents.

406

407   While a complete or quantitative oxygen budget of the OMZs is beyond the scope of this

408   investigation, it is interesting to put the synoptic oxygen fluxes for the EUC, the SCCs,

409   and the ICCs presented here into a qualitative context by estimating the diffusive oxygen

410   fluxes into the OMZs for comparison, and by assessing the bulk oxygen consumption

411   rate implied by summing the (admittedly rough and incomplete) advective and diffusive

17

412   fluxes. The mass transport estimated for the EUC, the SCCs and the ICCs (Table 1) at

413   and west of 125°W is about 30×10^9 kg s^{-1}. If we assume that the mass flux of these

414   eastward currents is returned by the adjacent westward currents, and that the typical

415   oxygen concentration difference between eastward and westward flows is about 20 μmol

416   kg^{-1} (Figure 8), we get a net oxygen flux of 0.6×10^6 mol s^{-1}.

417

418   We make rough estimates of the diffusive fluxes through the climatological 60 μmol kg^{-1}

419   surface surrounding the tropical Pacific OMZ.   We first compute the gradients

420   perpendicular to this surface, then apply a representative diapycnal diffusion coefficient

421   of 1×10^{-5} m^2 s^{-1} [*Ledwell et al.*, 1998] to their vertical component, and a representative

422   isopycnal diffusion coefficient of 500 m^2 s^{-1} [*Davis*, 2005] to their lateral component.

423   While *Davis* [2005] found a much larger value for the zonal component of lateral

424   diffusivity near the equator, we use 500 m^2 s^{-1}, more characteristic of off-equatorial

425   regions in his analysis, since using that larger equatorial value would arguably double-

426   count much of the fluxes estimated from synoptic zonal currents above.   Integrating

427   these products over the surface area results in a vertical oxygen flux of 0.4×10^6 mol s^{-1},

428   mostly through the top surface where the vertical gradients are large.   The lateral

429   diffusive flux, similarly estimated, is 0.8×10^6 mol s^{-1}, somewhat larger than either the

430   zonal advective flux or the vertical diffusive flux.

431

432   The mass of the tropical Pacific OMZs (water between 30°S and 30°N with oxygen

433   concentrations < 60 μmol kg^{-1}) is about 16×10^{18} kg. Dividing the sum of the flux

434   estimates made above by the OMZ mass gives an oxygen utilization rate (OUR) of about

435   4 μmol kg^{-1} a^{-1}. We are aware of no other OUR estimates specific to the OMZ, but this

436   result compares favourably to 6.6 to 3.2 μmol kg^{-1} a^{-1}, the range corresponding to 25.5 <

437   $\sigma_\theta < 26.6$ kg m^{-3} inferred for the subtropical North Pacific [*Sonnerup et al.*, 1999]. This

438   exercise suggests zonal current oxygen fluxes as estimated here may make a significant

439   contribution to the OMZ oxygen budget, along with vertical and lateral diffusive fluxes.

440   Hence changes of these zonal fluxes could contribute to OMZ temporal and spatial

441   variations.

442

443   Multi-decadal oxygen time series are difficult to construct from the few observations

444   available. However, by combining historical equatorial oxygen measurements with

445   recent TAO measurements, we find oxygen decreasing by roughly 0.5 μmol kg^{-1} a^{-1} over

446   the last 30 years, averaged within 3 degrees of the Equator and east of the Dateline, and

447   from 200-700 m as well as for a corresponding density layer. The scatter is very large,

448   however, and it remains to be seen whether the signal is decadal variability such as the

449   slowdown and recent rebound of the subtropical cell in the upper Pacific Ocean

450   [*McPhaden and Zhang,* 2004], or a longer-term climate change.

451

461

462 **References**

463

464 Boyer, T. P., J. I. Antonov, H. Garcia, D. R. Johnson, R. A. Locarnini, A. V. Mishonov,

465   M. T. Pitcher, O. K. Baranova, and I. Smolyar (2006), World Ocean Database

466   2005, Chapter 1: Introduction, NOAA Atlas NESDIS 60, Ed. S. Levitus, U.S.

467   Government Printing Office Washington D.C., 182 pp., DVD.

468 Curry, R., (1996), HydroBase − A database of hydrographic profiles and tools for

469   climatological analysis, Woods Hole Oceanographic Institution, Tech. Report,

470   WHOI-96-01, 50 pp.

471 Davis, R. E., (2005), Intermediate-depth circulation of the Indian and South Pacific

472   Oceans measured by autonomous floats, *J. Phys. Oceanogr.*, *35*, 683–707.

473 Eden, C., and A. Timmermann (2004), The influence of the Galapagos Islands on

474   tropical temperatures, currents and the generation of tropical instability waves,

475   *Geophys. Res. Lett., 31,* L15308, doi:10.1029/2004GL020060.

476 Eldin, G., (1983), Eastward flows of the South Equatorial Central Pacific, *J. Phys.*

477   *Oceanogr., 13,* 1461–1467.

478 Emerson, S., Y. W. Watanabe, T. Ono, and S. Mecking (2004), Temporal trends in

479   apparent oxygen utilization in the upper pycnocline of the North Pacific: 1980-

480   2000, *Jour. Oceanogr.*, 60, 139–147.

481 Fiedler, P.C., and L. D. Talley (2006), Hydrography of the eastern tropical Pacific: A

482   review, *Prog. Oceanogr., 69,* 143–180.

483 Fine, R., K. A. Maillet, K. F. Sullivan, and D. Willey (2001), Circulation and ventilation

484   flux of the Pacific Ocean, *J. Geophys. Res., 106*(C10), 22,159–22,178.

485   Firing, E., S. E. Wijffels, and P. Hacker (1998), Equatorial subthermocline currents

486   across the Pacific, *J. Geophys. Res., 103*(C10), 21,413–21,423.

487   Fuenzalida, R., W. Schneider, J. Garces-Vargas, L. Bravo, and C. Lange (2009), Vertical

488   and horizontal extension of the oxygen minimum zone in the eastern South

489   Pacific Ocean, *Deep-Sea Res. II, 56,* 1027–1038.

490   Hanawa, K., and L. D. Talley (2001), Mode Waters, in *Ocean circulation and climate:*

491   *Observing and modelling the global ocean*, edited by G. Siedler, J. Church and J.

492   Gould, pp. 373–386, Academic Press, New York.

493   Hayes, S. P., J. M. Toole, and L. J. Mangum (1983), Water-mass and transport

494   variability at 110°W in the equatorial Pacific, *J. Phys. Oceanogr., 13*, 153–168.

495   Johnson, G. C., and D. W. Moore (1997), The Pacific subsurface countercurrents and an

496   inertial model, *J. Phys. Oceanogr., 27*, 2448–2459.

497   Johnson, G. C., B. M. Sloyan, W. S. Kessler, and K. E. McTaggart (2002), Direct

498   measurements of upper ocean currents and water properties across the tropical

499   Pacific during the 1990s, *Prog. Oceanogr., 52*, 31–61.

500   Joos, F., G.-K. Plattner, T. F. Stocker, A. Körtzinger, and D. W. R. Wallace (2003),

501   Trends in marine dissolved oxygen: Implications for ocean circulation changes

502   and the carbon budget, *EOS Trans. AGU, 84,* 197–204.

503   Karstensen, J., L. Stramma, and M. Visbeck (2008), Oxygen minimum zones in the

504   eastern tropical Atlantic and Pacific Oceans, *Prog. Oceanogr., 77*, 331–350.

505   Keeling, R. F, and H. Garcia (2002), The change in oceanic O_2 inventory associated with

506   recent global warming, *Proceedings of the National Academy of Sciences of the*

507   *United States of America, 99*, 7848–7853.

508   Kessler, W. S., (2006), The circulation of the eastern tropical Pacific: A review, *Prog. in*

509   *Oceanogr., 69*, 181–217.

510   Ledwell, J. R., A. J. Watson, and C. S. Law (1998), Mixing of a tracer in the pycnocline,

511   *J. Geophys. Res.*, 103, 21,499–21,529.

512   Luyten, J. R., J. Pedlosky, and H. Stommel (1983), The ventilated thermocline, *J. Phys.*

513   *Oceanogr., 13,* 292–309.

514   Matear, R. J., and A.C. Hirst (2003), Long-term changes in dissolved oxygen

515   concentrations in the ocean caused by protracted global warning, *Global*

516   *Biogeochem. Cycles, 17*, 1125, doi:10.1029/2002GB001997.

517   McPhaden, M. J., and D. Zhang (2004), Pacific Ocean circulation rebounds. *Geophys.*

518   *Res. Lett., 31*, L18301, doi:10.1029/2004GL020727.

519   Montgomery, R. B., and E. D. Stroup (1962), Equatorial waters and currents at 150°W

520   in July–August 1952, *The Johns Hopkins Oceanographic Studies I,* 68 pp.

521   Oschlies, A., K. G. Schulz, U. Riebesell, and A. Schmittner (2008), Simulated 21st

522   century's increase in oceanic suboxia by CO2-enhanced biotic carbon export,

523   *Global Biogeochem. Cycles, 22*, GB4008, doi:10.1029/2007GB003147.

524   Paulmier, A., and D. Ruiz-Pino (2009), Oxygen minimum zones (OMZs) in the modern

525   ocean. *Prog. Oceanogr., 80*, 113–128.

526   Rowe, G. D., E. Firing, and G. C. Johnson (2000), Pacific Equatorial Subsurface

527   Countercurrent Velocity, Transport, and Potential Vorticity, *J. Phys. Oceanogr.,*

528   *30,* 1172–1187.

529   Schlitzer, R., (2007), Ocean data view, http://odv.awi.de.

530   Schott, F. A., J. P. McCreary and G. C. Johnson (2004), Shallow overturning circulation

531   of the tropical-subtropical oceans, in *Earth's Climate: The Ocean Atmosphere*

532   *Interaction,* edited by C. Wang, S.-P. Xie, and J.A. Carton, pp. 261–304, AGU,

533   Washington, D.C.

534   Sonnerup, R. E., P. D. Quay, and J. L. Bullister (1999), Thermocline ventilation and

535   oxygen utilization rates in the subtropical North Pacific based on CFC

536   distributions during WOCE, *Deep-Sea Res. I, 46*, 777–805.

537   Stramma, L., P. Brandt, J. Schafstall, F. Schott, J. Fischer, and A. Körtzinger (2008a),

538   The oxygen minimum zone in the North Atlantic south and east of the Cape

539   Verde Islands, *J. Geophys. Res., 113,* C04014, doi:10.1029/2007JC004369.

540   Stramma, L., G. C. Johnson, J. Sprintall, and V. Mohrholz (2008b), Expanding oxygen-

541   minimum zones in the tropical oceans, *Science, 320*, 655–658.

542   Tsuchiya, M., (1975), Subsurface countercurrents in the eastern equatorial Pacific

543   Ocean, *J. Mar. Res. 33 (Suppl.),* 145–175.

544   Tsuchiya, M., and L. D. Talley (1998), A Pacific hydrographic section at 88°W: Water-

545   property distribution, *J. Geophys. Res., 103*(6), 12,899–12,918.

546   Von Storch, H., and F.W. Zwiers (1999), *Statistical Analysis in Climate Research*,

547   Cambridge University Press, Cambridge, pp. 371-374.

548   Whitney, F. A., H. J. Freeland, and M. Robert (2007), Persistently declining oxygen

549   levels in the interior waters of the eastern subarctic Pacific, *Prog. Oceanogr., 75*,

550   179–199.

551   Wijffels, S. E., J. M. Toole, H. L. Bryden, R. A. Fine, W. J. Jenkins, and J. L. Bullister

552   (1996), The water masses and circulation at 10°N in the Pacific, *Deep-Sea Res. I,*

553   *43*, 501–544.

554   Wong, A. P. S., and G. C. Johnson (2003), South Pacific Eastern Subtropical Mode

555   water, *J. Phys. Oceanogr.*, *33*, 1493–1509.

556   Wunsch, C., (1996), *The ocean Circulation Inverse Problem*, Cambridge University

557   Press, Cambridge, pp. 113-119.

558   Wyrtki, K., (1962), The oxygen minima in relation to ocean circulation, *Deep-Sea Res.*,

559   *9*, 11–23.

560   Wyrtki, K., and B. Kilonsky (1984), Mean water and current structure during the

561   Hawaii-to-Tahiti shuttle experiment, *J. Phys. Oceanogr.*, *14*, 242–254.

562

562
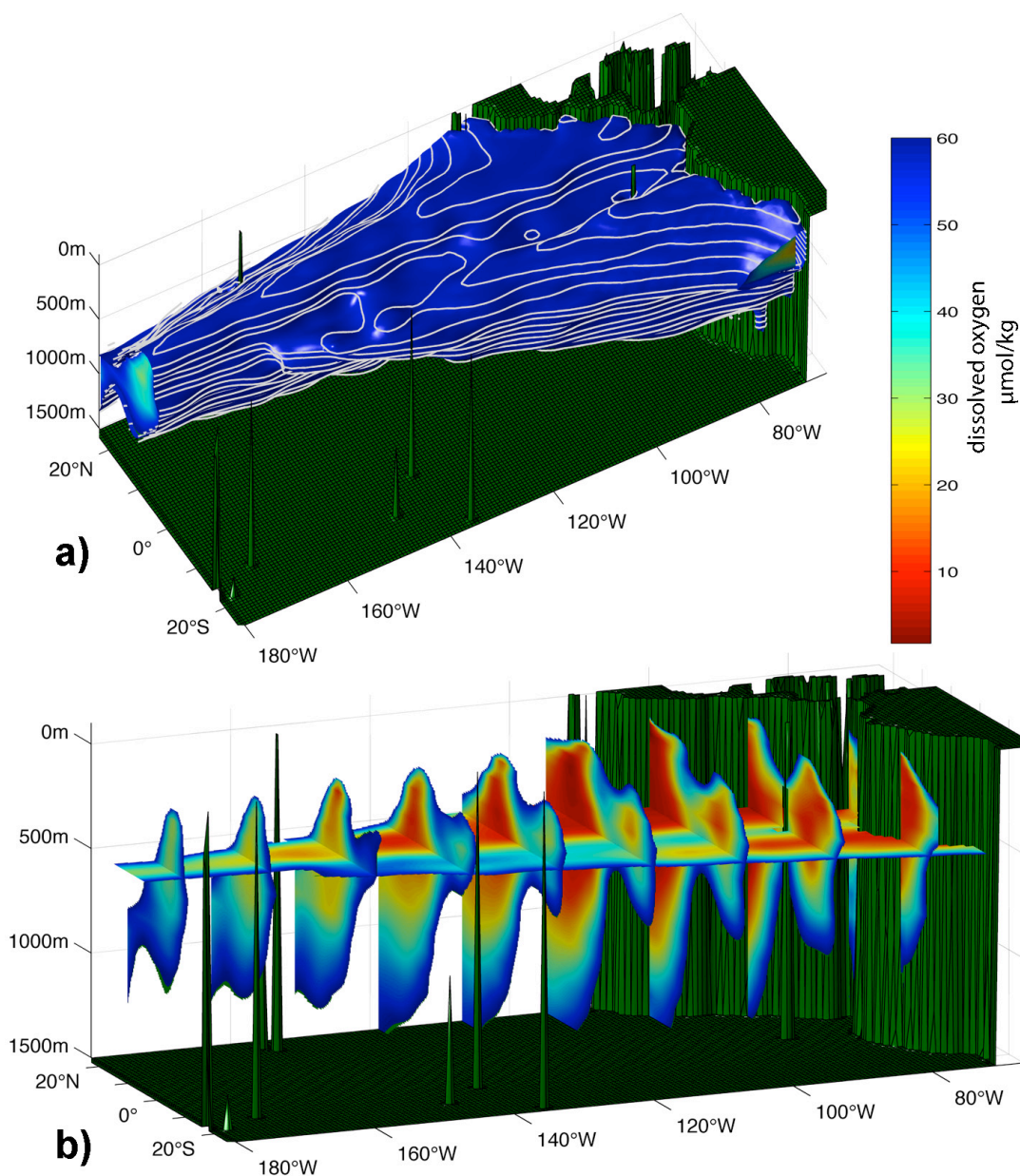
563

564   **Figure 1.** 3-D visualizations of the North and South Pacific eastern oxygen-minimum

565   zones (OMZs) displaying a) the 60 μmol kg⁻¹ oxygen isosurface with 50-m depth

566   contours as white lines and b) vertical and horizontal slices with oxygen concentrations

567   < 60 μmol kg⁻¹ color shaded as indicated in the bottom color bar. Data base is the

568   WOA05 1-degree mean climatology.

569
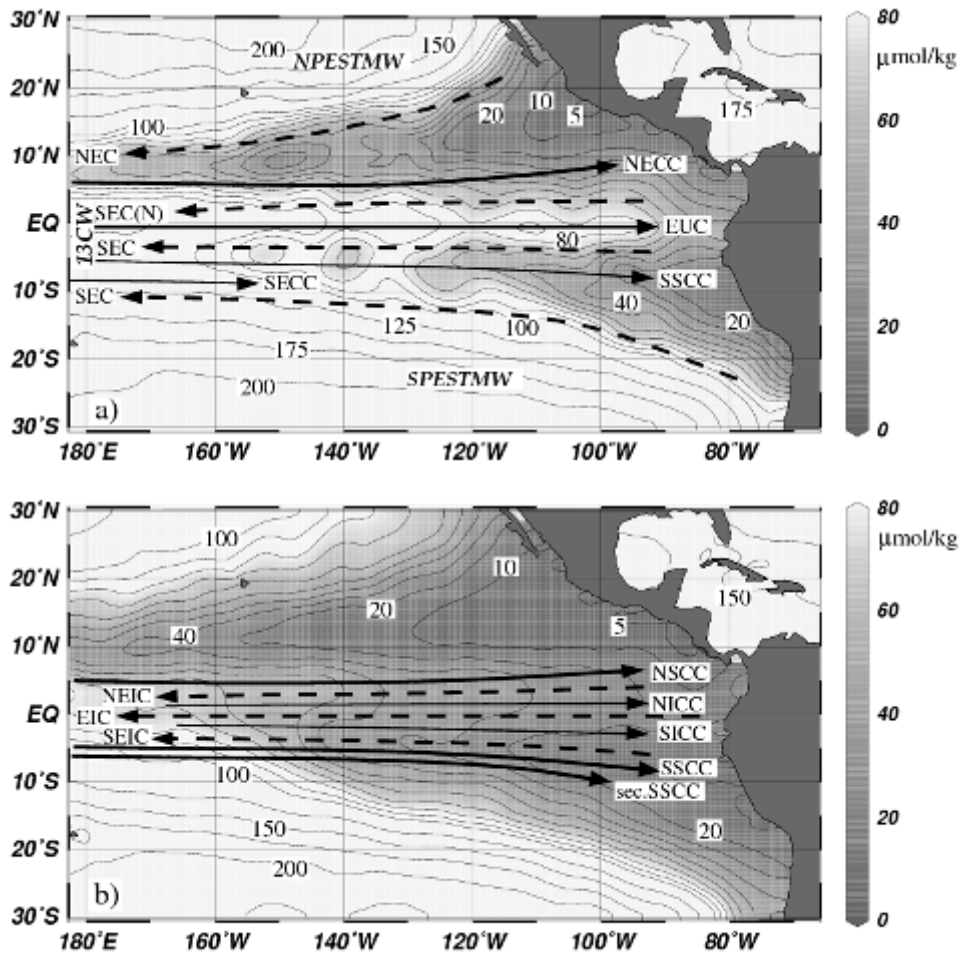
Figure 2. Eastern tropical Pacific distribution of mean dissolved oxygen on a) $\sigma_\theta = 26.3$ kg m^{-3}, located at about 150 to 300 m and b) $\sigma_\theta = 26.8$ kg m^{-3}, located at about 350 to 450 m. Contours are shown for 5 μmol kg^{-1}, at 10 μmol kg^{-1} increments from 10 to 100 μmol kg^{-1} and at 25 μmol kg^{-1} increments for values above 100 μmol kg^{-1}. WOA05 mean climatology is plotted using Ocean Data View software [*Schlitzer,* 2007]. Currents indicated for a) the near surface layers and b) the subpycnocline layers include the North Equatorial Current (NEC), the North Equatorial Countercurrent (NECC), the northern and main branches of the South Equatorial Current (SEC(N), SEC), the Equatorial Undercurrent (EUC), the Northern and Southern Subsurface Countercurrents (NSCC, SSCC), the South Equatorial Countercurrent (SECC), the North and South

26

580   Intermediate Currents (NICC, SICC), the Equatorial Intermediate Countercurrent (EIC),

581   the North and South Equatorial Intermediate Currents (NEIC, SEIC) as well as the

582   secondary band of the SSCC (sec.SECC). These currents are not necessarily found

583   exactly on the two isopycnals shown. For their typical vertical locations see Figures 3 to

584   7. Schematic locations of 13°C Equatorial Water (13CW) and the South and North

585   Pacific Eastern Subtropical Mode Water (SPESTMW, NPESTMW) are also indicated.

586   The NEC and SEC carry NPESTMW and SPESTMW westward, while in the eastern

587   shadow zones containing modified 13CW [*Fiedler and Talley,* 2006] not much

588   exchange takes place.

589

590
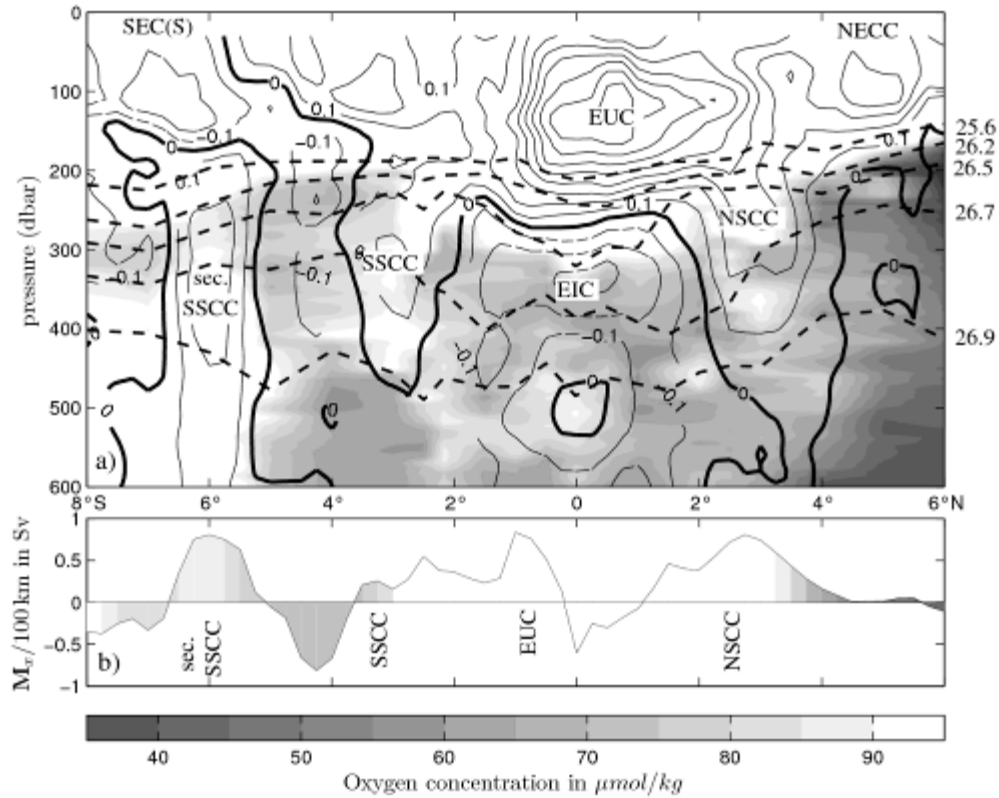
Figure 3. a) Oxygen distribution (gray shading for 35 to 90 μmol kg^{-1}), selected

isopycnals (dashed lines), and ADCP-measured zonal velocity (black contours at 0.1 m

s^{-1} intervals, positive eastward) along 170°W in July 2004.   The southern branch of the

South Equatorial Current (SEC(S)), the Equatorial Undercurrent (EUC), the Southern

and Northern Subsurface Countercurrent (SSCC, NSCC), the North Equatorial

Countercurrent (NECC). and the North Equatorial Intermediate Current (NEIC) are

indicated. b) Transport in Sv/100 km for $26.2 < \sigma_\theta < 26.5$ kg m^{-3}, gray shaded by the
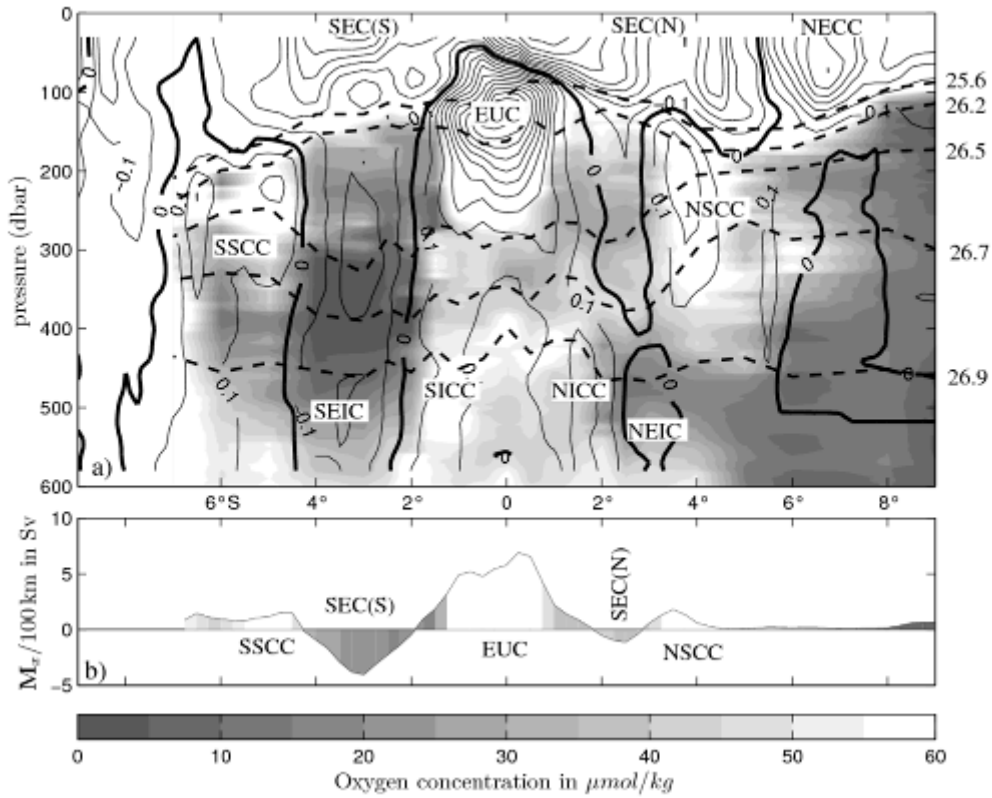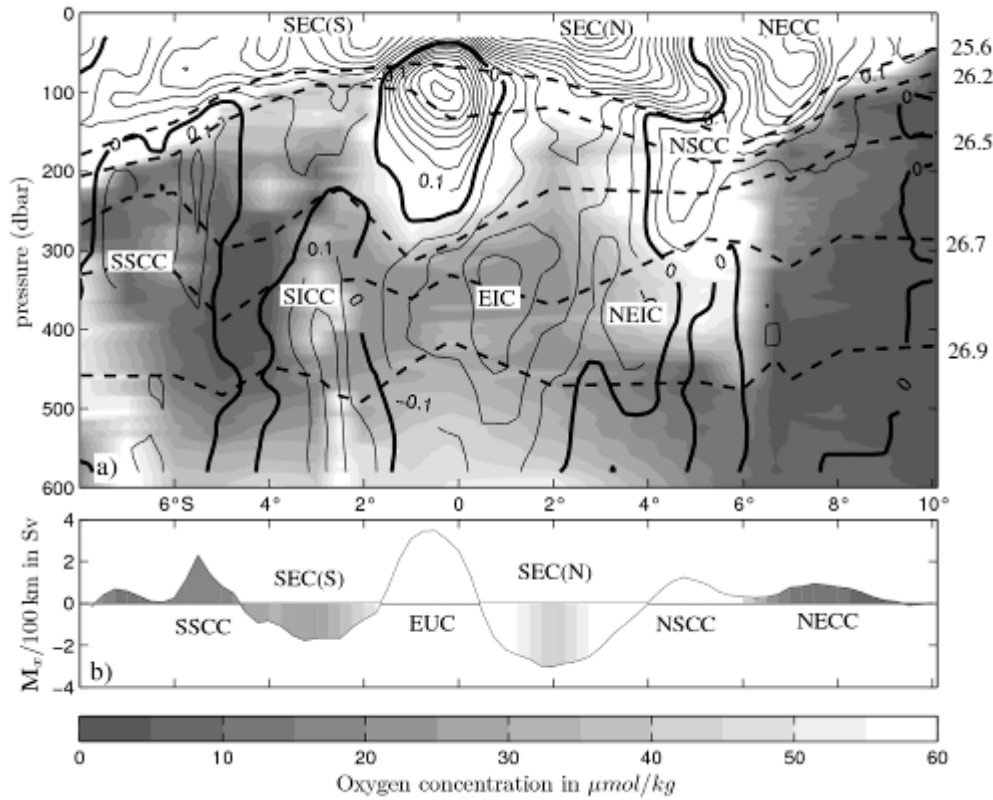
layer-mean oxygen concentration.

Figure 4. a) Oxygen distribution (gray shading for 0 to 55 μmol kg^{-1}), selected isopycnals (dashed lines), and ADCP-measured zonal velocity (black contours at 0.1 m s^{-1} intervals, positive eastward) along 140°W in January 2006. Current markings follow Figure 3, adding the northern branch of the South Equatorial Current (SEC(N)) as well as, the South and North Intermediate Countercurrents (SICC, NICC). b) Transport in Sv/100 km for 26.2 < σ$_\theta$ < 26.5 kg m^{-3}, gray shaded by the layer mean oxygen concentration.

607

Figure 5. a) Oxygen distribution (gray shading for 0 to 55 μmol kg^{-1}), selected

isopycnals (dashed lines), and ADCP-measured zonal velocity (black contours at 0.1 m

s^{-1} intervals, positive eastward) along 125°W in January–February 2006. Current

markings follow Figure 3. b) Transport in Sv/100 km for $26.2 < \sigma_\theta < 26.5$ kg m^{-3}, gray

shaded by the layer mean oxygen concentration.

613

Figure 6. a) Oxygen distribution (gray shading for 0 to 55 μmol kg^{-1}), selected

isopycnals (dashed lines), and ADCP-measured zonal velocity (black contours at 0.1 m

s^{-1} intervals, positive eastward) along ~95°W in October–November 2003. Current

markings follow Figure 3, adding the Costa Rica Dome (CRD). b) Transport in Sv/100

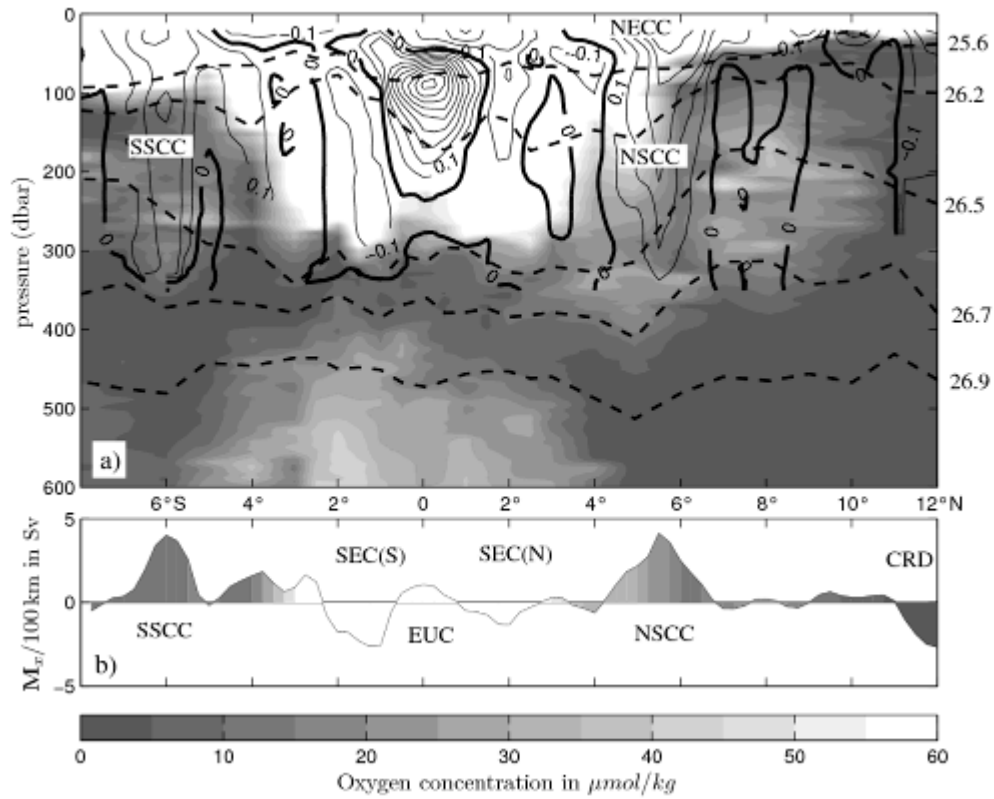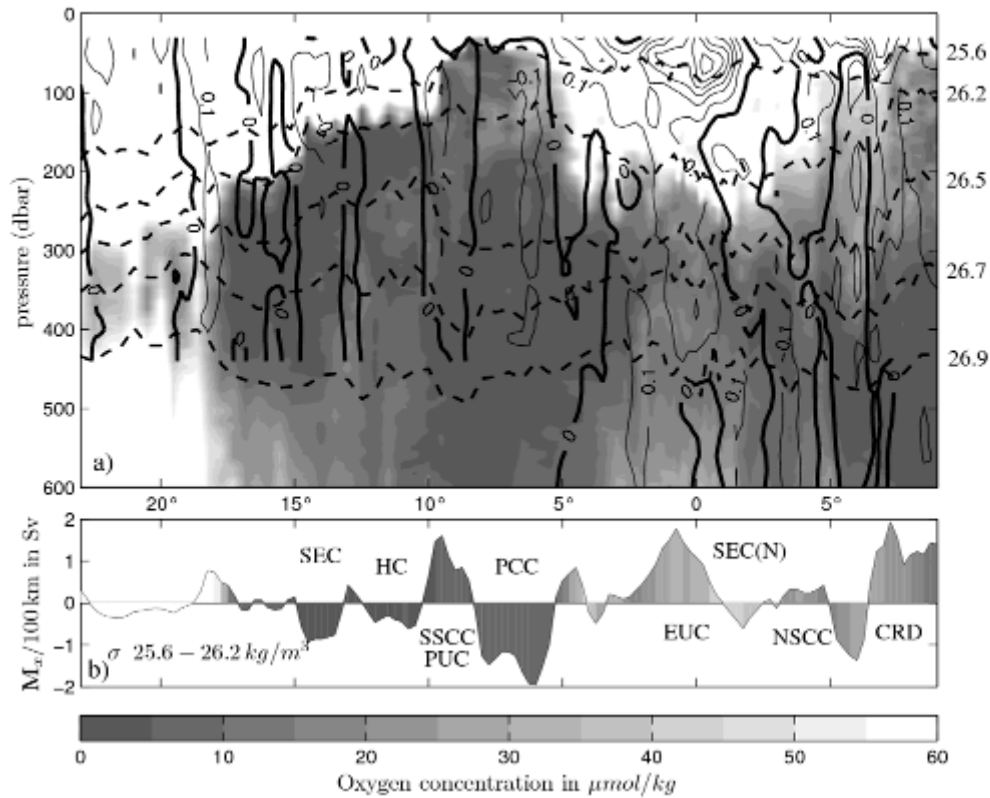km for $26.2 < \sigma_\theta < 26.5$ kg m^{-3}, gray shaded by the layer mean oxygen concentration.

619

Figure 7. a) Oxygen distribution (gray shading for 0 to 55 μmol kg^{-1}), selected
isopycnals (dashed lines), and ADCP-measured zonal velocity (black contours at 0.1 m
s^{-1} intervals, positive eastward) along ~85°W in March–April 1993. North of 5°S
currents below 450 dbar are from the lowered ADCP. Current markings follow Figure 3,
adding the Humboldt Current (HC), the Peru Chile Undercurrent as a continuation of the
SSCC, the Peru-Chile Current (PCC), and the Costa Rica Dome (CRD). b) Transport in
Sv/100 km for $26.2 < \sigma_\theta < 26.5$ kg m^{-3}, gray shaded by the layer mean oxygen
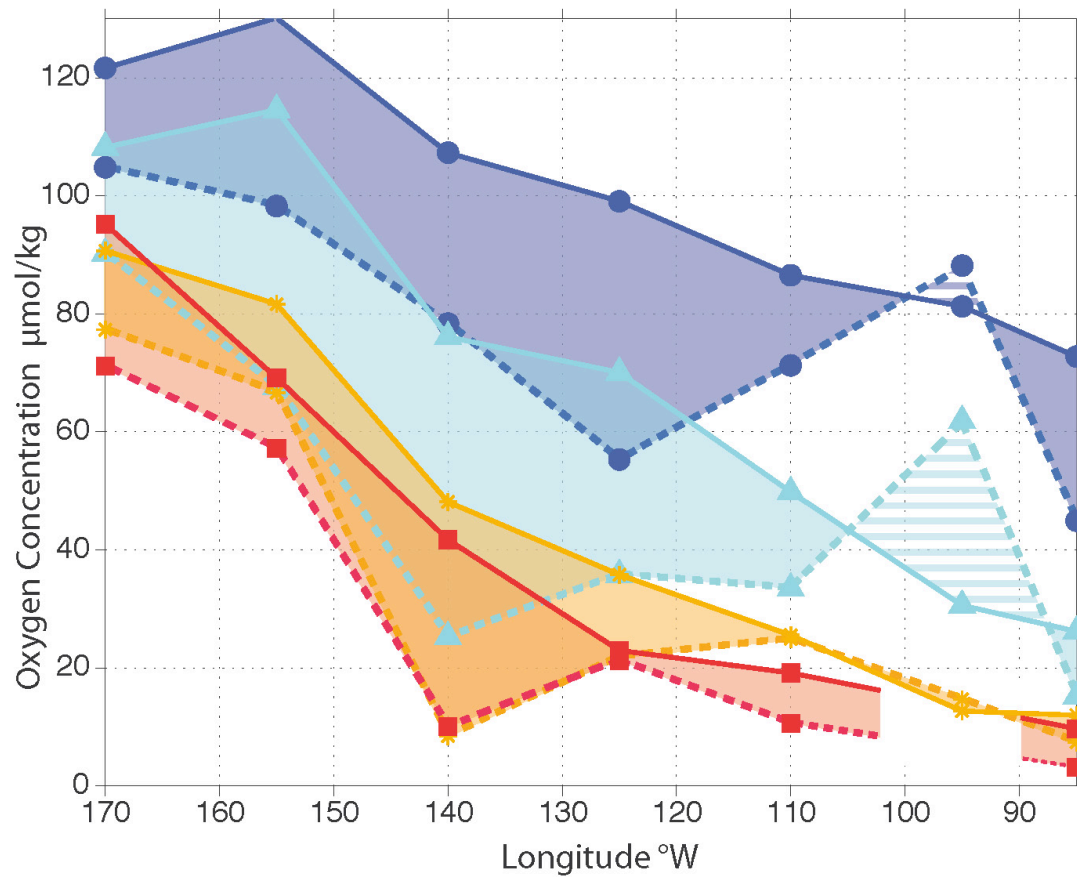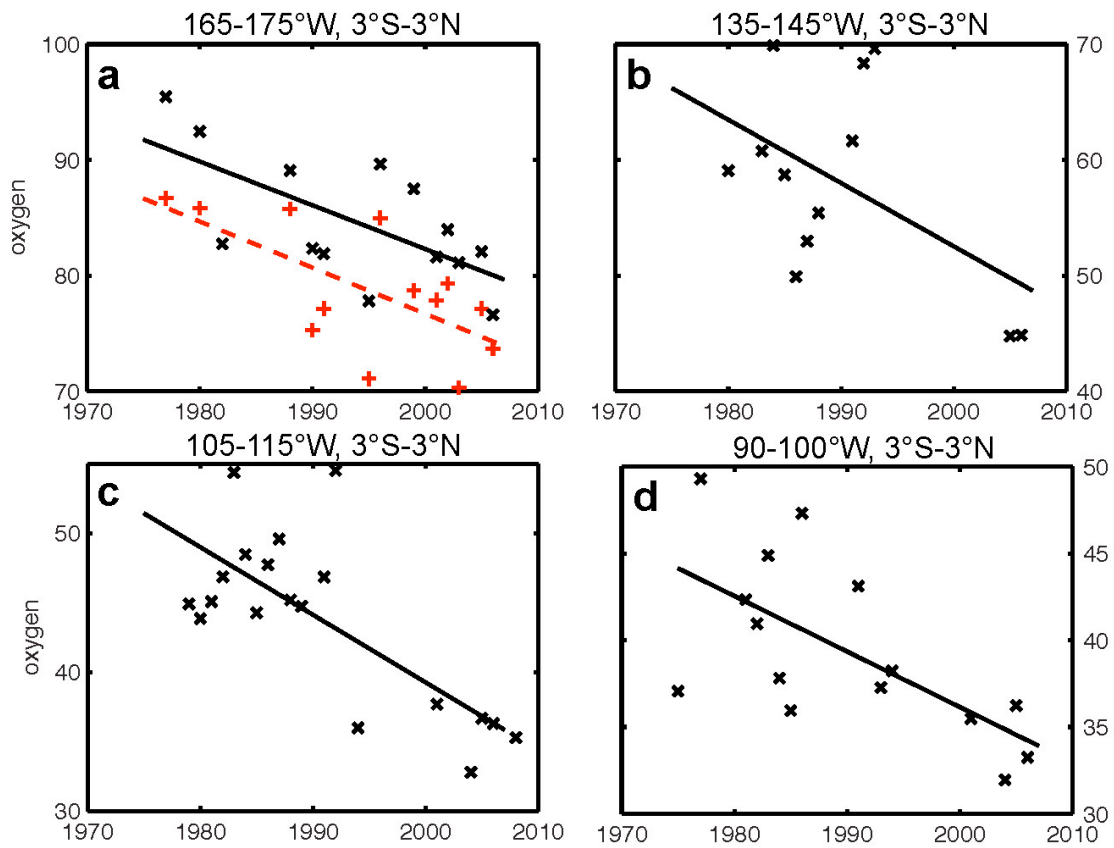concentration.

629

Figure 8. Eastward (solid lines) and westward (broken lines) oxygen concentration (oxygen flux divided by mass transport; flux/Tr in μmol kg^{-1}) versus longitude for selected density layers between 8°S and 8°N, except 170°W: 8°S-6°N and 140°W: 7°S-8°N for $25.6 < \sigma_\theta < 26.2$ kg m^{-3} (blue, circles), $26.2 < \sigma_\theta < 26.5$ kg m^{-3} (cyan, triangles), $26.5 < \sigma_\theta < 26.7$ kg m^{-3} (orange, stars), and $26.7 < \sigma_\theta < 26.9$ kg m^{-3} (red, squares). Values at 95°W for $26.5 < \sigma_\theta < 26.7$ kg m^{-3} and at 85°W for $26.7 < \sigma_\theta < 26.9$ kg m^{-3} are incomplete as the ADCP did not sample the deepest portions of these layers over the entire section.

638

639

Figure 9. Time series of annual mean 200–700 m dissolved oxygen concentrations (x's) since 1975 (in μmol kg^{-1}) with linear fits (solid lines). Trend values and their 95% confidence intervals from the fits are given in Table 2. Areas analyzed are between 3°S and 3°N at a) 165 to 175°W, b) 135 to 145°W, c) 105 to 115°W, and d) 95 to 105°W. In a) the time series for the isopycnal layer σ_θ=26.2-27.18 kg m^{-3} is included (+'s) with a linear fit (dashed line).

646

647

648   Table 1. Eastward mass transports (Tr in 10^9 kg s^{-1}), oxygen fluxes (10^3 mol s^{-1}) and

649   oxygen concentration (oxygen flux divided by mass transport; flux/Tr in µmol kg^{-1}) in a)

650   the EUC for 26.2 < σ_θ < 26.5 kg m^{-3} between 2°S and 2°N, b) the SSCC and the NSCC

651   for σ_θ = 26.2 < σ_θ < 26.9 kg m^{-3} and c) the SICC and NICC from σ_θ = 26.7 kg m^{-3} to 600

652   dbar.

653

654   a)

Section/time (mm/yy)	EUC-Tr	EUC-flux	flux/Tr
170°W 07/04	1.9	238.7	125
155°W 06-07/04	5.3	615.8	116
140°W 01/06	15.6	1263.8	81
125°W 01-02/06	6.5	634.0	97
110°W 12/07-01/08	21.1	1287.4	61
95°W 10-11/03	1.4	136.3	97
85°W 03-04/93	3.4	97.0	29

664

665

666

667

668   b)

Section/time (mm/yy)	SSCC: area	Tr	flux	flux/Tr	NSCC: area	Tr	flux	flux/Tr
170°W 07/04	8°S-2°S	9.6	951.4	99	2°N-5°N	8.9	792.6	89
155°W 06-07/04	8°S-3°S	3.1	261.0	84	2°N-6°N	3.8	316.9	83
140°W 01/06	8°S-4°S	9.1	434.3	48	3°N-7°N	8.9	496.5	56
125°W 01-02/06	8°S-4°S	7.8	138.8	18	3°N-7°N	6.7	377.2	56
110°W 12/07-01/08	8°S-3°S	9.0	206.9	23	3°N-8°N	12.7	390.5	31
85°W 03-04/93	11°S-7°S[*]	3.0	17.1	6	2°N-6°N	0.8	18.6	23

676   [*] shallow ADCP, lower boundary at $\sigma_\theta = 26.8$ kg m^{-3}.

678   c)

Section/time (mm/yy)	SICC: area	Tr	flux	flux/Tr	NICC: area	Tr	flux	flux/Tr
155°W 06-07/04	3°S-0°S	3.6	234.3	65	1°N-3°N	0.6	38.6	64
140°W 01/06	3°S-0°S	5.0	250.2	50	0°N-3°N	8.1	349.4	43
125°W 01-02/06	4°S-1°S	6.7	234.9	35	2°N-5°N	1.4	37.9	27
110°W 12/07-01/08	3°S-0°S	11.2	388.7	35	0°N-4°N	17.1	458.1	27
85°W 03-04/93	5°S-0°S	8.7	115.1	13	0°N-4°N	4.3	53.9	13

688 Table 2. Temporal oxygen trends (μmol kg^{-1} a^{-1}) and their 95% confidence intervals

689 from linear fits for a 200 to 700 m layer (Figure 9) with percentages of the total variance

690 (var) accounted for by those linear trends and the degrees of freedom (dof) used in the

691 uncertainty estimates.   The same parameters for an isopycnal layer, $26.2 < \sigma_\theta < 27.18$ kg

692 m^{-3}, that roughly spans the 200–700-m depth range.

693

Area	200–700 m				$26.2 < \sigma_\theta < 27.18$ kg m^{-3}			
	trend	confidence	var	dof	trend	confidence	var	dof
3°S-3°N, 165-175°W	-0.38	+/-0.30	43%	12.0	-0.40	+/-0.26	43%	11.0
3°S-3°N, 135-145°W	-0.55	+/-0.88	26%	7.1	-0.46	+/-0.79	20%	7.8
3°S-3°N, 105-115°W	-0.49	+/-0.24	54%	15.7	-0.52	+/-0.31	56%	11.6
3°S-3°N, 90-100°W	-0.32	+/-0.22	42%	13.0	-0.21	+/-0.28	22%	9.5